

2. Zweite Transformationsart

Übergang vom System (x_0, y_0, z_0) zum System (x_1, y_1, z_1) und vom System (x^{p-1}, y^{p-1}, z^{p-1}) zum System (x^p, y^p, z^p) für p = 2 bis z.

Die allgemeinen Transformationsgleichungen lauten für p = 1:

(x)_1 = (x)_0 * (x'_1 r_0) + (y)_0 * (x'_1 y_0) + (z)_0 * (x'_1 z_0) - a'_{0,1}
(y)'_1 = (x)_0 * (y'_1 r_0) + (y)_0 * (y'_1 y_0) + (z)_0 * (y'_1 z_0) - b'_{0,1}
(z)'_1 = (x)_0 * (z'_1 r_0) + (y)_0 * (z'_1 y_0) + (z)_0 * (z'_1 z_0) - c'_{0,1}

und für p = 2 bis z:

(x)^p = (x)^{p-1} * (x'^p r_{p-1}) + (y)^{p-1} * (x'^p y_{p-1}) + (z)^{p-1} * (x'^p z_{p-1}) - a'^{p-1,p}
(y)^p = (x)^{p-1} * (y'^p r_{p-1}) + (y)^{p-1} * (y'^p y_{p-1}) + (z)^{p-1} * (y'^p z_{p-1}) - b'^{p-1,p}
(z)^p = (x)^{p-1} * (z'^p r_{p-1}) + (y)^{p-1} * (z'^p y_{p-1}) + (z)^{p-1} * (z'^p z_{p-1}) - c'^{p-1,p}

Hierin gelten für p = 2 bis z für die Richtungsosinus der Einheitsvektoren r^p, y^p, z^p gegen die Einheitsvektoren r^{p-1}, y^{p-1}, z^{p-1} den Gl. (61) völlig entsprechende Gleichungen, nur daß in (61) mit Ausnahme der Größen r_0, y_0, z_0 überall anstelle der ungestrichelten Größen r_{p-1}, y_{p-1}, z_{p-1} die entsprechenden gestrichelten Größen r^p, y^p, z^p, r^{p-1}, y^{p-1}, z^{p-1} zu schreiben sind.

Sodann erhält man:

a'_{0,1} = (x_1)_0 * (x'_1 r_0) + (y_1)_0 * (x'_1 y_0) + (z_1)_0 * (x'_1 z_0)
b'_{0,1} = (x_1)_0 * (y'_1 r_0) + (y_1)_0 * (y'_1 y_0) + (z_1)_0 * (y'_1 z_0)
c'_{0,1} = (x_1)_0 * (z'_1 r_0) + (y_1)_0 * (z'_1 y_0) + (z_1)_0 * (z'_1 z_0)
(x_2)^0_1 = (x_2)^0_0 * (x'_1 r_0) + (y_2)^0_0 * (x'_1 y_0) + (z_2)^0_0 * (x'_1 z_0) - a'_{0,1}
(y_2)^0_1 = (x_2)^0_0 * (y'_1 r_0) + (y_2)^0_0 * (y'_1 y_0) + (z_2)^0_0 * (y'_1 z_0) - b'_{0,1}
(z_2)^0_1 = (x_2)^0_0 * (z'_1 r_0) + (y_2)^0_0 * (z'_1 y_0) + (z_2)^0_0 * (z'_1 z_0) - c'_{0,1}
a'_{1,2} = (x_2)^0_1 * (x'_2 r_1) + (y_2)^0_1 * (x'_2 y_1) + (z_2)^0_1 * (x'_2 z_1)
b'_{1,2} = (x_2)^0_1 * (y'_2 r_1) + (y_2)^0_1 * (y'_2 y_1) + (z_2)^0_1 * (y'_2 z_1)
c'_{1,2} = (x_2)^0_1 * (z'_2 r_1) + (y_2)^0_1 * (z'_2 y_1) + (z_2)^0_1 * (z'_2 z_1)
(x_3)^0_1 = (x_3)^0_0 * (x'_1 r_0) + (y_3)^0_0 * (x'_1 y_0) + (z_3)^0_0 * (x'_1 z_0) - a'_{0,1}
(x_3)^0_1 = (x_3)^0_0 * (y'_1 r_0) + (y_3)^0_0 * (y'_1 y_0) + (z_3)^0_0 * (y'_1 z_0) - b'_{0,1}
(x_3)^0_1 = (x_3)^0_0 * (z'_1 r_0) + (y_3)^0_0 * (z'_1 y_0) + (z_3)^0_0 * (z'_1 z_0) - c'_{0,1}
(x_3)^0_2 = (x_3)^0_1 * (x'_2 r_1) + (y_3)^0_1 * (x'_2 y_1) + (z_3)^0_1 * (x'_2 z_1) - a'_{1,2}
(y_3)^0_2 = (x_3)^0_1 * (y'_2 r_1) + (y_3)^0_1 * (y'_2 y_1) + (z_3)^0_1 * (y'_2 z_1) - b'_{1,2}
(z_3)^0_2 = (x_3)^0_1 * (z'_2 r_1) + (y_3)^0_1 * (z'_2 y_1) + (z_3)^0_1 * (z'_2 z_1) - c'_{1,2}
a_{2,3} = (x_3)^0_2 * (x'_3 r_2) + (y_3)^0_2 * (x'_3 y_2) + (z_3)^0_2 * (x'_3 z_2)
b_{2,3} = (x_3)^0_2 * (y'_3 r_2) + (y_3)^0_2 * (y'_3 y_2) + (z_3)^0_2 * (y'_3 z_2)
c_{2,3} = (x_3)^0_2 * (z'_3 r_2) + (y_3)^0_2 * (z'_3 y_2) + (z_3)^0_2 * (z'_3 z_2)

Man erkennt auch hier bereits das Bildungsgesetz für die weiteren Formeln bis zur Berechnung von a_{z-1,z}, b_{z-1,z}, c_{z-1,z}. (Die Teile II-IV folgen)

Beam Displacement at Total Reflection:
The Goos-Hänchen Effect, III*

By Helmut K. V. Lotsch**

Institut für Theoret. Elektrotechnik, TH Aachen, Germany

Received 1 April 1970

Abstract

The paper is divided into four parts. Part I comprises the Introduction and the two chapters entitled "Reflection and Refraction of a Beam of Light" and "Total Reflection of an E-Polarized Beam". Part II treats the Goos-Hänchen effect in classical optics. The different descriptions are discussed and their results are compared with Wolter's measurements. Part III deals with the Goos-Hänchen effect in other branches of physics such as acoustics, quantum mechanics, plasma physics and nonlinear optics. The Schöck effect is introduced; further more the total reflection of diverging and converging waves is investigated. The final Part IV is devoted to several applications of the Goos-Hänchen effect, including the case of absorbing media. In addition, it contains the Summary and Conclusion, and the extensive list of references.

Inhalt

Strahlversetzung bei der Totalreflexion. III. Die vorliegende Arbeit ist in vier Teile unterteilt. Teil I umfaßt die Einleitung und die beiden Kapitel "Reflexion und Brechung eines Lichtstrahles" und "Totalreflexion eines E-polarisierten Lichtstrahles". Teil II behandelt den Goos-Hänchen-Effekt in der klassischen Optik. Die verschiedenen Beschreibungen werden besprochen und ihre Ergebnisse mit den Messungen von Wolter verglichen. Teil III befaßt sich mit dem Goos-Hänchen-Effekt in anderen Zweigen der Physik, nämlich der Akustik, der Quanten-Mechanik, der Plasma-Physik und der nichtlinearen Optik. Der Schöck-Effekt wird eingeführt; ebenso wird die Totalreflexion divergierender und konvergierender Wellen untersucht. Der abschließende Teil IV ist einigen Anwendungen des Goos-Hänchen-Effektes, einschließlich dem Fall absorbierender Medien, gewidmet. Außerdem enthält er die Zusammenfassung und Schlussbetrachtung und das ausführliche Literaturverzeichnis.

4. The Goos-Hänchen Effect in Other Branches of Physics

The Goos-Hänchen effect, originally discovered in classical optics, is encountered in other branches of physics, too. The physical connection becomes apparent when considering the totally reflected beam a superposition of plane waves whose mutual phase relations are sensitive functions of their angles of incidence. As we recall from (20b), the phase shift suffered by

* Dissertation approved by the Faculty of Electrical Engineering at the Technical University of Aachen, translated int. English.
** Author's address: Antonietos Division of North American Rockwell, Anaheim, California 92808.

a plane wave at total reflection depends upon its angle of incidence, particularly near the critical angle for total reflection. The individual plane-wave components are, therefore, superimposed with mutual phase relations which not only differ from those of the incident beam but also change drastically as the angle of incidence approaches the critical angle for total reflection. The change in the mutual phase relations of the plane-wave components may be interpreted as the physical origin of the *Goos-Hänchen* effect. This interpretation is, of course, consistent with that based on the flow of light energy, which is emphasized in the present paper.

The theory of total reflection cast into the notation of either acoustics, quantum mechanics or plasma physics is briefly outlined in Sections 4.1 through 4.3. Bearing the above discussion in mind, we treat the plane-wave theory and, when considering a beam, derive the *Goos-Hänchen* effect from it by differentiating the phase shift with respect to the angle of incidence, as shown in Section 3.2. Needless to say, the formulas so obtained represent good approximations only at angles close to the critical angle for total reflection where the *Goos-Hänchen* effect is significant. They also fail for the same reason right at the critical angle and in the limit of grazing incidence.

Section 4.4 treats the *Goos-Hänchen* effect in terms of nonlinear optics, assuming an optically less-dense medium which is nonlinear. It is shown that the drastic increase approaches the critical angle for total reflection, provides a novel method to demonstrate the light penetration into the less-dense medium. A simple method for calculating the nonlinear *Goos-Hänchen* effect of light harmonics is outlined. Its basic idea is to lump the nonlinear mechanism into a phase shift of the reflected (harmonic) wave so that the physical optics treatment of Section 3.2 is applicable in the denser linear medium.

The formalism of total reflection is also discovered in the theory of diffraction gratings when the wavelength becomes larger than the grating constant [48]. This special case is gaining importance in optics, but will not be treated separately in this chapter.

4.1 Acoustics

The propagation of sound is likewise described by the wave equation (2b), only the speed of light must be replaced by the much slower speed of sound. Consequently a sound wave, when encountering an obstacle, undergoes diffraction, reflection, and refraction like an optical wave; illustrations may be found in textbooks (e.g., [49]). Although a homogeneous and isotropic medium with simple boundary conditions may be assumed, the acoustical problem is rather involved in general. In contrast to optics the acoustical field, broadly speaking, can support not only a transverse or shear wave, but also a longitudinal or compressional wave. Both satisfy the wave equation (2b) with appropriate velocities. The longitudinal and shear waves, although propagating independently in an unbounded medium, may be coupled by boundary conditions at interfaces. An important example to be discussed below is the Rayleigh wave. It consists of two inhomogeneous waves, one longitudinal and one transverse, which propagate along the boundary of the

half-space with identical velocities, but attenuate differently with depth. On the boundary, these components cancel the stress which they produce. Instead of attempting to treat the complicated problem in general, let us indicate the physics involved by selecting a few simple cases of particular interest.

Gases and most liquids can only support longitudinal waves but not shear waves since they do not exhibit shearing stress. Simplification is, therefore, obtained in cases where gas and/or liquid is involved. The simplest case of all consists of two media without shearing stress adjoining one another along a plane interface. An incident wave is reflected and refracted analogously to an optical wave treated above. The fact that the field is described by longitudinal waves here and by transverse waves there is immaterial since both satisfy the wave equation (2b) with appropriate velocities. Consequently the laws of reflection and refraction apply and the amplitudes of the reflected and refracted waves are given by Fresnel's formulas. The corresponding formulas for compressional waves are obtained either from (13) if n is replaced by $(\rho_1 v_1 / \rho_2 v_2)$ or from (16) if n is replaced by $(\rho_2 v_2 / \rho_1 v_1)$, where ρ and v denote the density and velocity in the respective medium (see Fig. 3), [22a]. Total reflection takes place as the angle of incidence exceeds the critical angle $\Phi_l = \arcsin(n_l)$, where $n_l = v_1/v_2$ is the acoustical index of refraction, the subscript l referring to "longitudinal". The angle-dependent phase shift

$$\delta_l = 2 \arctan \left(\frac{\rho_1 / \sqrt{\sin^2 \Phi_l - \sin^2 \Phi_l}}{\rho_2 \cos \Phi_l} \right) \quad (49)$$

produces, when considering a beam of sound, the *Goos-Hänchen* effect as in optics. On substituting (49) into (43), we obtain the expression derived by Schoch [22a] for the beam displacement in the case of two media without shearing stress

$$D_l = \frac{A}{2\pi} \frac{\sin \Phi_l}{\sqrt{\sin^2 \Phi_l - \sin^2 \Phi_l}} \left[\frac{\rho_{12}(1 - \sin^2 \Phi_l)}{\cos^2 \Phi_l + \rho_{12}^2 (\sin^2 \Phi_l - \sin^2 \Phi_l)} \right], \quad (50)$$

where A stands for the acoustical wavelength in the first medium and ρ_{12} is a shorthand for the ratio (ρ_1/ρ_2) .

The problem next in complexity deals with the case of a compressional wave which impinges upon a solid occupying the lower half-space in Fig. 3 liquid. Under these conditions, the incident energy of the longitudinal wave is partitioned between a reflected longitudinal wave and the refracted longitudinal and shear waves ([22a] and [50]). The latter waves propagated in the solid with different velocities; the longitudinal wave is always faster than the shear wave which itself is faster than the incident wave. At normal incidence, a refracted shear wave does not exist, so the energy is partitioned between the reflected and refracted longitudinal waves. As the angle of incidence is increased, some energy goes into the refracted shear wave until the critical angle for the refracted longitudinal wave, i.e., the condition where

the angle of refraction equals 90 degrees, is approached. At this angle (say, 15°), all the energy is theoretically reflected back into the first medium. At higher angles, the refracted shear wave receives a fairly large percentage of the incident energy until it also approaches its critical angle, say, at 30°. In this somewhat simplified picture, the incident energy would be totally reflected at all larger angles. At both critical angles the reflected wave undergoes phase shifts which may be interpreted, when considering a beam of sound, as producing *Goos-Hänchen* effects.

When the possibility of surface waves is admitted to the interpretation of the foregoing problem, a more complex situation exists. A major change in reflection occurs at an angle of incidence just beyond that which produces critical refraction of the shear wave. At this angle, the phase velocity of the incident wave projected onto the interface is identical with that of the "Rayleigh wave" in the solid. Although the surface wave referred to here may differ slightly from a true Rayleigh wave (characterized by a vacuum/solid boundary), the velocities are almost identical. There is one important difference between liquid/solid surface-waves and vacuum/solid surface-waves due to the vastly distinct densities of a liquid and a vacuum. At low megahertz frequencies, the latter may travel over long distances with relatively little attenuation. However, surface waves at a liquid/solid interface are rapidly damped due to radiation of a compressional wave into the liquid. In any case, the reflected wave undergoes a large phase shift of as much as 2π in the immediate neighborhood of that angle $\Phi_R = \arcsin(v_1/v_R)$, v_R being the velocity of the Rayleigh wave, [22b]. For the two examples water/aluminum and xylene/aluminum, to be discussed below, the angle Φ_R amounts to 31° and 27°, respectively.

Considering a beam of sound, the sudden phase shift at the angle Φ_R gives rise to an abrupt shift of the reflection center in the amount of, [22]

$$\xi_s = \frac{1}{\pi Q_1} \sqrt{\frac{2Q_2}{r(r-s)} \frac{1 + 6s^2(1-q) - 2s(3-2q)}{s(s-1)}}, \quad (51)$$

where the various quantities are defined as $q = (v_{gr}/v_{gl})^2$, $r = (v_{gr}/v_{1l})^2$, and $s = (v_{gr}/v_R)^2$, v_{gr} and v_{gl} being the velocities of the longitudinal and shear waves in the solid (medium 2). The quantity s represents the only one positive root of the Rayleigh equation

$$4s \sqrt{1-s} \sqrt{q-s} + (1-2s)^2 = 0$$

in the range $(0 < q < 0.5)$. It depends slightly upon Poisson's constant of the solid and is confined to the range (1.1, 1.3); for example, $s = 1.15$ for aluminum. That is, as q varies from 0 to 0.5, the phase velocity of the Rayleigh wave varies monotonically from $0.87v_{gr}$ to $0.96v_{gr}$. It can be shown that the Rayleigh wave does not exhibit phase-velocity dispersion.

The phenomenon described by (51) is physically analogous to the *Goos-Hänchen* effect, but not identical with it in a strict sense. The *Goos-Hänchen* effect, although significant merely in the neighborhood of the critical angle for total reflection, takes place in the entire range of total reflection, whereas this phenomenon arises only at the angle Φ_R or in a very narrow angle range about Φ_R . To our knowledge, Schoch originally predicted [22a] and later demonstrated [22b] this phenomenon. In recognition of his work, therefore, we introduce the term "the Schoch effect"; the subscript S in (51) already refers to "Schoch". Obviously, the Schoch effect can be expressed equally as a beam displacement Δ , as a depth of penetration ζ , or as a shift of the reflection center ξ . These interpretations are related by (32), translating the letters D, X, and Z into Greek.

The Schoch effect is so large, namely $\xi_s = 21.4\lambda$ for water/aluminum and 33.4λ for xylene/aluminum, that it becomes directly visible in a Schlieren method [51] at ultrasound. Illustrations for a xylene/aluminum interface are presented in Fig. 12 at 16 MHz (a) and 5.5 MHz (b), having the wavelengths of 0.08 mm (a) and 0.24 mm (b) in xylene. The central figure of each set shows the case of incidence at Φ_R , whereas those on both sides were taken at a slightly smaller and a slightly larger angle of incidence, respectively. The Schoch effect is quite pronounced in the two central figures and absent in all others; the beam is shifted by 2.7 mm at 16 MHz and by nearly its full width

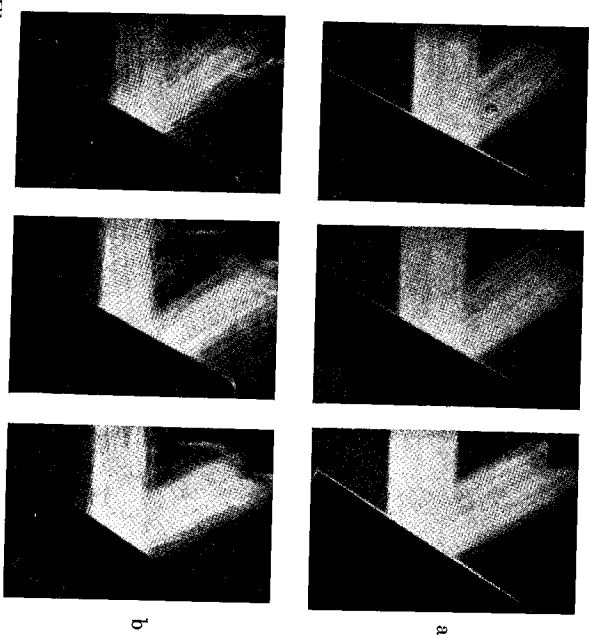


Fig. 12. Illustrating the Schoch effect at a xylene/aluminum interface for 16 MHz (a) and 5.5 MHz (b). [22b]. The horizontally incident beam of sound, having the width of 12 mm, is shifted only at the angle Φ_R , shown in the central figures. The angle of incidence is respectively slightly smaller and slightly larger than Φ_R in the two outer pictures of each set.

at 5.5 MHz. Obviously, the beam contour is more blurred the lower the frequency due to diffraction.

Needless to say, delimiting the second medium to some finite thickness rather than having it occupy the entire half-space introduces a further degree of complexity. In a manner similar to planar dielectric waveguides [38] normal modes, the so-called Lamb waves [52], are excited in addition, [22a]. Interaction between the incident beam and all the waves being generated in the limited second medium can lead, under certain circumstances, to displacements of the transmitted beam as well. A discussion of these phenomena would exceed the scope of the present paper; the interested reader is referred elsewhere (e. g., [30a] and [53]).

4.2 Quantum Mechanics

The wave-particle duality of light bears out the fact that a beam of particles, when being totally reflected at a potential barrier, should also exhibit the *Goos-Hänchen* effect. *Hora* [24] investigated this problem on the basis of quantum mechanics. He solved Schroedinger's equation separately for the two half-spaces of Fig. 3 with the respective potential energies V_1 and V_2 , and matched the boundary conditions across the interface at $z = 0$. An incident wave with the energy $E > V_2 > V_1$ is totally reflected if the angle of incidence exceeds the critical angle Φ_{QM} defined by $\sin \Phi_{QM} = \sqrt{(E - V_2) / (E - V_1)}$, undergoing the phase shift δ_r of (20b). Utilizing a plane-wave expansion for the reflected beam of particles and following *Schoch's* method of asymptotic evaluation [22a], *Hora* obtained for the beam displacement

$$\Delta_H = \frac{h}{2\pi \sqrt{2m(E - V_1)}} \frac{d}{d\varphi} |\delta_r|, \quad (52)$$

where the subscript H refers to "*Hora*", h is Planck's constant, and m denotes the mass of a particle. Introducing the de Broglie wavelength

$$\lambda_{dB} = h / \sqrt{2m(E - V_1)}$$

Obviously, *Hora's* results also valid only for angles close to the critical angle for total reflection and fails in the limit of grazing incidence. *Renard* [13] later showed that extending *Hora's* treatment with the principle of particle conservation leads to the general expression (34) or (40a).

4.3 Plasma Physics

The reflection and refraction of electromagnetic waves at flat plasma boundaries have been investigated extensively (see, e.g., [54]). The propagation within the plasma, occupying the lower half-space in Fig. 3, is describable by a complex dielectric constant if the wavelength is substantially larger than the average distance between transparent electrons or ions. The upper half-space may either be filled with a transparent medium or represent a vacuum, confining the plasma to the lower half-space by a magnetic field. The former case is

more general and sketched in this section; the results for the latter are straightforwardly derivable from those to be presented. The dielectric constant of a plasma is smaller than that of vacuum. Total reflection is, therefore, anticipated in some angle range. This problem and the associated *Goos-Hänchen* effect when considering a beam was thoroughly investigated by *Schilling* [23] on the basis of *Wolter's* theory outlined in Section 3.2. We shall freely draw on *Schilling's* mathematical results and refer to the original work for a detailed discussion.

The complex dielectric constant of a homogeneous and isotropic plasma occupying the second medium can be written in the following manner

$$\epsilon_2 = \epsilon_2' - i4\pi\sigma_2/\omega = K_2' - iK_2'', \quad (53a)$$

where ϵ_2' and σ_2 denote the permittivity and electric conductivity of the plasma, respectively, and ω is the angular frequency of the electromagnetic wave. The quantities K_2' and K_2'' are determined by the characteristics of the plasma, i.e.,

$$K_2' = 1 - \frac{\omega_p^2}{\omega^2} \frac{1}{1 + \nu^2/\omega^2} \quad \text{and} \quad K_2'' = \frac{\nu \omega_p^2}{\omega \omega^2} \frac{1}{1 + \nu^2/\omega^2}, \quad (53b)$$

where the angular frequency of the plasma oscillation, if the effective collision frequency $\nu \ll \omega$, is given by

$$\omega_p = \sqrt{4\pi N e^2/m}$$

with N being the concentration of electrons, $e = 4.80 \times 10^{-10}$ egs being the charge of an electron and $m = 9.11 \times 10^{-28}$ g being its mass. The oscillation of the heavy ions as well as near-field forces are, for our purpose, negligible in the plasma frequency.

The first medium of Fig. 3 is not specified explicitly. For reasons of generality, the assumption is made that the dielectric constant of this medium is complex as well and can be expressed by (53a), interchanging the subscripts. If representing another plasma, the quantities K_1' and K_1'' are written in a manner similar to (53b).

Total reflection takes place if the angle of incidence exceeds the critical angle Φ_p defined by $\sin \Phi_p \approx \sqrt{K_2'/K_1'}$ for $K_1'' \ll 1$ and $K_2'' \ll 1$. For angles near Φ_p , *Schilling* [23a] obtained the following approximations for the shift of the reflection center, assuming $K_1'' \ll K_1'$ and $K_2'' \ll K_2'$

$$\Delta_{S_L} = \frac{\lambda_1}{\pi} \frac{K_1'}{K_1'} \sqrt{\frac{K_2'}{2(K_1' - K_2')}} \sqrt{\frac{s \pm \sqrt{1 + s^2}}{(1 + s^2)(K_1'K_2'' - K_2'K_1'')}} \quad (54a)$$

and

$$\Delta_{S_U} = \Delta_{S_L} / \sin^2 \Phi_p, \quad (54b)$$

where the subscript S refers to 'Schilling', and the shorthand s is given by

$$s = \frac{K_2' - K_1' \sin^2 \varphi}{K_2'' - K_1'' \sin^2 \varphi}.$$

In (54a) the upper sign is used if $K_1' K_2'' > K_2' K_1''$, and the lower sign in all other cases.

It can be shown [23a] that $X_{S\perp}$ assumes its maximum value

$$X_{S\perp} |_{\max} =$$

$$\frac{A_1}{2\pi} \sqrt{\frac{1}{27}} \frac{K_1' \sqrt{K_2'}}{\sqrt{2(K_1' - K_2') |K_1' K_2'' - K_2' K_1''|}} \approx 1.14 X_{S\perp} |_{\varphi = \Phi_p} \quad (55a)$$

not at Φ_p but at

$$\Phi_{\max} = \Phi_p + \frac{\sqrt{3}}{6} \frac{|K_1' K_2'' - K_2' K_1''|}{K_1' \sqrt{K_2'} (K_1' - K_2')} \quad (55b)$$

Hence, if absorptive losses are taken into account and thus $K_1'' \neq 0$, the *Goos-Hänchen* effect is most pronounced at an angle of incidence slightly larger than critical angle for total reflection. It is interesting to note that a small, but nonvanishing conductivity of the first medium does lead to an enhancement of the *Goos-Hänchen* effect. The maximum enhancement is obtained for $K_1'' = K_1' K_2'' / K_2'$, yielding $\Phi_{\max} = \Phi_p$. If K_1'' exceeds this value, the *Goos-Hänchen* effect decreases drastically since partial reflection takes over.

In the case of two absorbing plasmas on both sides of the interface at $z = 0$, the critical angle Φ_p is defined by $\sin \Phi_p \approx \sqrt{\frac{\omega^2 - \omega_{p2}^2}{\omega^2 - \omega_{p1}^2}}$. This relation reveals that the critical angle depends upon the angular frequency of the incident wave. For a given angle of incidence, the critical angular frequency to obtain total reflection is derived from the above relation to be

$$\Omega^2 \geq \frac{\omega_{p2}^2 - \omega_{p1}^2 \sin^2 \varphi}{\cos^2 \varphi} \quad (56)$$

The maximum shift of the reflection center is deduced from (55a), yielding

$$X_{S\perp} |_{\max} = \frac{A_1}{2\pi} \sqrt{\frac{1}{27}} \sqrt{\frac{\omega^2 - \omega_{p2}^2}{2(\omega_{p2}^2 - \omega_{p1}^2)}} \frac{\omega^2 - \omega_{p1}^2}{\sqrt{\frac{p_2^2}{\omega} (\omega_{p2}^2(\omega^2 - \omega_{p1}^2)) - \frac{p_1^2}{\omega} (\omega_{p1}^2(\omega^2 - \omega_{p2}^2))}} \quad (57)$$

Assuming that the first medium is represented by a lossy dielectric with the electric conductivity σ_1 , we obtain for the maximum shift of the reflection center from (55a)

$$X_{S\perp} |_{\max} = \frac{A_1}{2\pi} \sqrt{\frac{1}{27}} \frac{1}{\cos \Phi_p} \left(2 \frac{p_2}{\omega} \frac{\omega_{p2}^2}{\omega^2 - \omega_{p2}^2} - \frac{4\pi\sigma_1}{\epsilon_1' \omega} \right)^{-\frac{1}{2}} \quad (58)$$

The corresponding expressions for H polarization can be straightforwardly derived, according to (54b), from the above equations.

The various formulas presented in this section were discussed by *Schilling* [23] from different points of view. The reader is referred to the original work for details and further results. He is, however, cautioned against the rather optimistic predictions for the magnitude of the *Goos-Hänchen* effect at the immediate neighborhood of the critical angle for total reflection. *Schilling's* derivations rest upon the physical-optics theory outlined in Section 3.2, which does not hold right at the critical angle. We recall that *Armann* suggested to exclude the narrow angle range of $(\varphi - \Phi_p) \leq 0.3^\circ$.

Schilling [23] pointed out that the *Goos-Hänchen* effect can be utilized to diagnose a plasma. A beam with a narrow spectrum of frequencies, which impinges upon the plasma under the critical angle for total reflection, produces, after reflection, a blurred rather than a well-defined spot. This phenomenon, revealing the effect of dispersion, depends upon the absorptivity of the plasma. Its measurement provides a possibility to determine the plasma frequency or concentration of electrons as well as the effective collision frequency or temperature of the plasma.

Finally, it should be mentioned that the formulas presented also hold in the case of a magneto-active plasma [23d].

4.4 Nonlinear Optics

The advent of the laser producing a high-intensity beam of light made available a new method to demonstrate the *Goos-Hänchen* effect, as first recognized by *Lotsch* [3]. This method is readily understood on the basis of Fig. 3. We assume that the upper half space is occupied by an optically denser linear medium, whereas the lower half space is filled with a less-dense nonlinear medium. Then, if a laser beam impinges upon the interface from the linear medium, harmonics can be detected in the totally-reflected beam if and only if the laser beam can interact with the less-dense nonlinear medium. The *Goos-Hänchen* effect, interpreted as light penetration into the less-dense medium, suggests that light harmonics should essentially be observable only near the critical angle for total reflection according to Fig. 6. This phenomenon was experimentally demonstrated by *Bloembergen, Lee and Simon* at the second harmonics [4], and by *Bey, Giuliani and Rabin* at the third harmonics [5]. Some of their results are reproduced in Fig. 13 and 14.

Let us shed some light on the physics involved in this nonlinear phenomenon from the viewpoint of our linear treatment of the *Goos-Hänchen* effect.

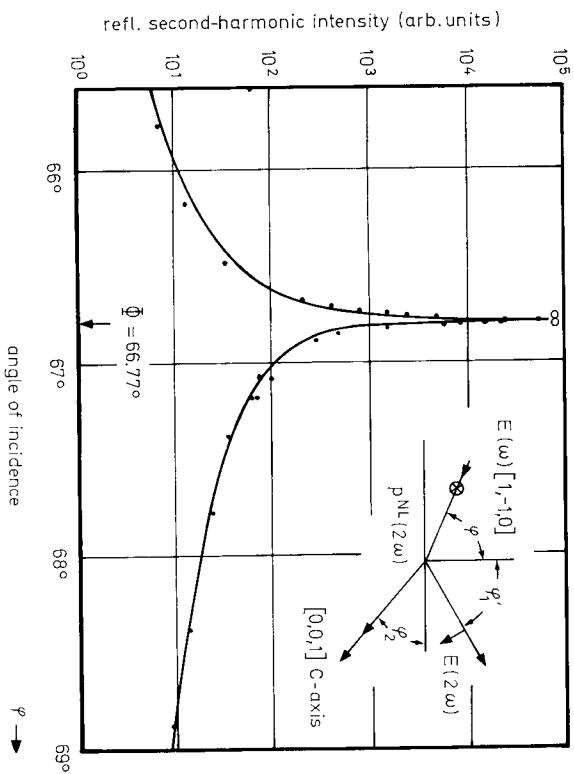


Fig. 13. The reflected second-harmonic intensity from KH_2PO_4 is exhibited in the neighborhood of the critical angle for total reflection, [4a]. The phase-matched direction is parallel to the interface. The incident beam at $\lambda = 9720\text{\AA}$ passes through the optically denser fluid 1-bromonaphthalene. The geometry for the nonlinear-optics experiment is shown in the inset. The drawn curve was calculated, and the points represent measurements. (Reproduction through the courtesy of N. Bloembergen et al., Harvard University, Cambridge, Massachusetts.)

We make the assumption that the amount of light harmonics generated is proportional to the path length along which the laser beam can interact with the nonlinear medium. In the ideal case of perfect phase matching [55], when the phase velocities of the fundamental and harmonic waves become equal, the intensity of the light harmonics even is proportional to the square of the path length [56]. A ray of light traces, according to Newton [2], a parabolic path through the less-dense medium¹⁰, as indicated in Fig. 1. The path or arc length L in the less-dense medium is given by

$$L_{\perp, \parallel} = \left[\frac{1}{\sin 2\varphi} + \frac{\tan \varphi}{2 \cos \varphi} \ln \left(\frac{\cos \varphi + 1}{\sin \varphi} \right) \right] D_{\perp, \parallel}, \quad (59)$$

where D stands for any one of the exact or approximate expressions stated in Chapter 3. Numerical results for L_{\perp}^2 , based upon either (34) or (36), are ¹⁰ This approximation is valid in the angle range in which the expressions (34) and (36) hold, as may be inferred from Fig. 17 of Reference 17. The resulting light ray propagation in the less-dense medium is, according to Maeker [17], expressible by assuming a rapid but continuous decrease in the index of refraction toward the less-dense medium.

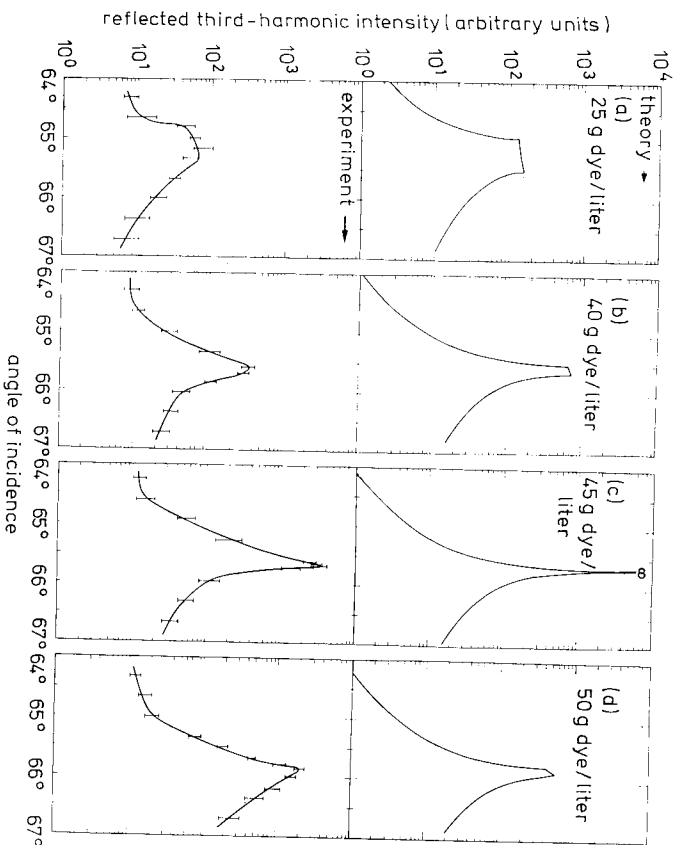


Fig. 14. The reflected third-harmonic intensity from a quartz/liquid interface is exhibited in the neighborhood of the critical angle for total reflection, [5c]. The incident beam was H polarized. The dye-liquid system consisted of fuchsin red dissolved in hexafluoroacetone sascquitydrate. Its concentration is stated for each case. (Reproduction through the courtesy of H. Rabin et al., Naval Research Laboratory, Washington, D. C.)

presented in Fig. 15, assuming the same critical angles for total reflection as in Fig. 5 and 6. The dotted portions of the curves for $\Delta \varphi = (\varphi - \Phi) < 0.25^\circ$ indicate that the validity of the respective expression for D is not necessarily guaranteed. Fig. 15 may be interpreted in terms of nonlinear optics. The light harmonics in the totally reflected beam, being proportional to the square of the path length in the case of perfect phase matching, should increase by several orders of magnitude as the angle of incidence approaches the critical angle, i.e., as $\Delta \varphi \rightarrow 0$. This conclusion is in agreement with the experimental results presented in Figs. 13 and 14. — As the critical angle for total reflection increases, the path length at a given $\Delta \varphi$ passes through a minimum somewhere in the vicinity of $\Phi = 55^\circ$; furthermore, the dependence upon polarization decreases. This fact explains the insignificant differences, with regard to polarization, noted by Bloembergen et al. [4b] and by Bey et al. [5c]. Those measurements were performed in the neighborhood of a critical angle which was approximately 65° . — The asymmetry around the critical angle for total reflection, exhibited by the curves of Figs. 13 and 14,

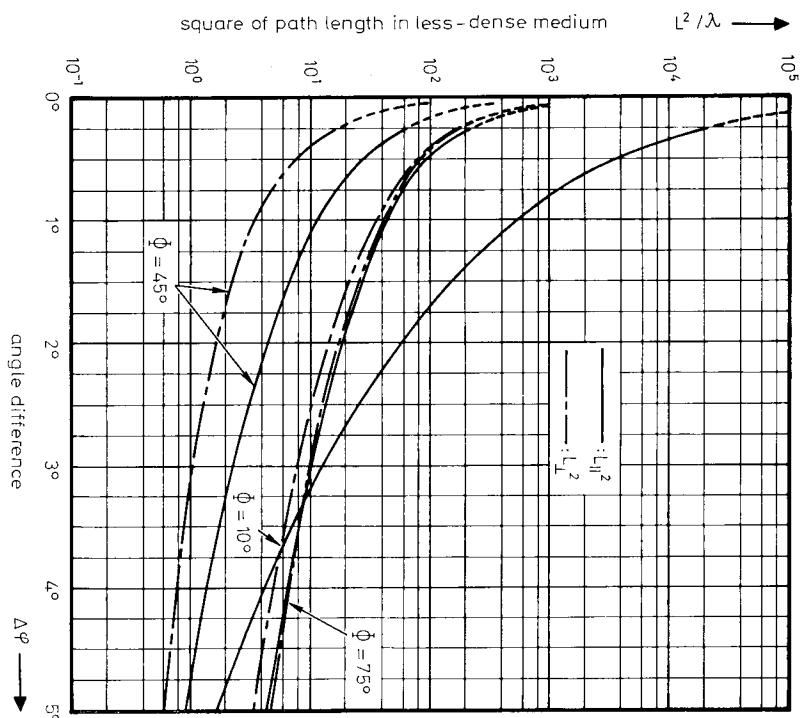


Fig. 15. Square of path length within the optically less-dense medium is plotted versus angle difference $\Delta\varphi = (\varphi - \Phi)$ for different values of the critical angle for total reflection Φ , as calculated by (39) with (34) and (36), respectively.

supports this interpretation further since the *Goos-Hänchen* effect vanishes in the region of partial reflection.

It is evident from above that the linear theory of the *Goos-Hänchen* effect describes physically the nonlinear generation of light harmonics at total reflection. In turn, the nonlinear-optics experiments substantiate the viewpoint of light penetration into the less-dense medium. This subject was under extensive investigation for several decades, as pointed out in the Introduction. Nevertheless, our linear interpretation of a nonlinear phenomenon should not be carried much further because of secondary effects such as, for example, phase mismatching and dispersion. In the general case of phase mismatching, the reflected light-harmonic intensity has two cusps at angles of incidence for which either the source or the harmonic wave undergoes critical refraction. As the phase-matched condition is approached, the two cusps move closer together and the peak intensity increases, as shown in Fig. 14 by varying the dye concentration. The singularity in the limit of

perfect phase matching must, however, be attributed to a mathematical artifact resulting from the plane-wave assumption for the incident beam. A similar difficulty in the linear case has been discussed in Section 3.3. The problem of phase matching is rather obvious in Reference 4b and is especially treated in Reference 5c.

We can also formulate a *Goos-Hänchen* effect for each light harmonic, as suggested by Bloembergen et al. [4b]11. Such a formulation would, in general, require a rather cumbersome extension of the derivation presented in Chapters 1 through 3 if the viewpoint of light penetration into the less-dense medium would be adopted. This is because a nonlinear phenomenon must be described by a nonlinear theory. Great simplification can, however, be obtained by lumping the nonlinear mechanism into a phase shift $\delta_{n\omega}(\varphi)$ of the reflected wave at the angular frequency $n\omega$, where $n = 2, 3, \dots$. Then, the *Goos-Hänchen* effect can be formulated, in a manner similar to the physical-optics treatment of Section 3.2, entirely in the denser linear medium, taking into account the phase shift due to the nonlinear mechanism. This phase shift may be derived from the nonlinear Fresnel formulas of Reference 57a, which are also utilized in References 4b and 5c. Using the approximation (43), the nonlinear-optics (NL) *Goos-Hänchen* effect for the n -th light harmonics is given by

$$D_{\text{NL}} = k_{n\omega} \frac{d}{d\varphi} |\delta_{n\omega}(\varphi)| \quad (60)$$

where $k_{n\omega}$ is the propagation constant for the angular frequency $n\omega$. It should be noted that the phase shift $\delta_{n\omega}(\varphi)$ accounts for the polarization under consideration.

The dispersion of the *Goos-Hänchen* effect can be readily written down in the following manner

$$\Delta D_{\text{NL}} = \frac{d}{d\varphi} [k_{\omega} |\delta_{\omega}(\varphi)| - k_{n\omega} |\delta_{n\omega}(\varphi)|]. \quad (61)$$

Needless to say, the phase shift $\delta_{n\omega}(\varphi)$ takes into account the problem of phase matching, as may be inferred from the extensive discussion of Reference 5c. It is straightforward to extend (60) and (61) to combination frequencies if the incident beam is nonmonochromatic.

5. Phenomena Related to the *Goos-Hänchen* Effect

This chapter is devoted to phenomena which bear some relationship to the *Goos-Hänchen* effect. We start out in Section 5.1 by generalizing the polarization of the parallel beam of light. In the case of arbitrary (linear or elliptic) polarization a beam displacement perpendicular to the plane of incidence is encountered, too. This displacement, theoretically postulated by *Kelovon* [29], is smaller than the *Goos-Hänchen* effect by roughly one order of magnitude.

¹¹ Meanwhile *Shih* [111] in collaboration with Bloembergen performed a detailed investigation of the *Goos-Hänchen* effect in nonlinear optics.

It is not clear to this author whether it has already been demonstrated by experiment.¹²

Up to this point, we have tacitly assumed that the beam of light is parallel and has emanated from a source at infinity, thus revealing the basic features of a plane wave. This assumption is now relaxed. Section 5.2 deals with the total reflection of a wave radiated by a source at finite distance. For reasons of generality, we speak of either a converging wave or a diverging wave and mean a (two-dimensional) cylindrical wave if a line source is assumed, or a (three-dimensional) spherical wave if a point source is assumed. It is shown that the reflected wave, if a diverging wave impinges upon a plane interface, is accompanied by a conical wavefront, a form of discontinuity familiar to us from fluid mechanics as a Mach cone, [49]. This wave is called *v. Schmidt's lateral wave*, in conformity with the electromagnetic nomenclature [26]. The terminology has been adopted in recognition of *v. Schmidt's* fundamental contribution to the physical understanding of lateral waves in acoustics and seismology, [25].

The beam of light, as illustrated in Fig. 4, strictly speaking, represents an idealization which can never be obtained exactly in practice. Diffraction introduced when cutting a plane wave by an aperture to form a beam may be insignificant, as in the theory of the *Goos-Hänchen* effect, but it is always present and modifies the beam. It can be demonstrated, at least in the border zone of the beam. The diffracted components of the beam-field may be visualized as cylindrical or spherical wavelets emanating from the edge of the aperture. Accordingly, we approximate a parallel beam with diffraction by a parallel beam-field upon which (diverging) diffraction waves are superimposed. That is to say, we supplement the theory of the *Goos-Hänchen* effect with the results of Section 5.2. This physical interpretation is treated in Section 5.3, pointing out the relevance of the diffraction waves to surface-wave phenomena.

5.1 Parallel Beam with Arbitrary Polarization

A parallel beam with arbitrary polarization is conveniently expressed, according to *Schilling* [18], by its degree of polarization, namely

$$P_e = \frac{A_{\perp}^2 - A_{\parallel}^2}{A_{\perp}^2 + A_{\parallel}^2} \quad \text{and} \quad P_r = \frac{R_{\perp}^2 - R_{\parallel}^2}{R_{\perp}^2 + R_{\parallel}^2}$$

for the incident (e) and the reflected (r) beam, respectively. Then, the beam displacement in the plane of incidence is given by

$$D = \frac{\lambda}{4\pi} \left[(1 - P_r) \frac{d}{dp} |\operatorname{arcc} R_{\parallel}| + (1 + P_r) \frac{d}{dp} |\operatorname{arcc} R_{\perp}| \right] \quad (62)$$

¹² It should be noted that the spot movement reported in [58a] is, although not clearly expressed, in the plane of incidence.

and the shift of the reflection center perpendicular to the plane of incidence by

$$Y_F = -\frac{\lambda}{2\pi} \operatorname{ctng} \left[\sqrt{1 - P_r^2} \sin(|\operatorname{arcc} R_{\perp}| - |\operatorname{arcc} R_{\parallel}| + \gamma) + \sqrt{1 - P_e^2} \sin \gamma \right], \quad (63)$$

where the subscript F refers to "Fedorov", and γ denotes the phase difference between the two orthogonally polarized wave components. The beam displacement D depends only upon the angle of incidence and is linearly proportional to the degree of polarization. For either E or H polarization (62) reduces to Artmann's expression (43).

The shift Y_F was first postulated by *Fedorov* [29], although it could have been extracted from the Poynting vectors in the early papers of *Boguslavski* [27] and *Wiegrefe* [28]. This shift is maximum if both incident and reflected beams are circularly polarized in the same direction. If the incident beam is linearly polarized, Y_F has a maximum for circular polarization of the reflected beam. In the limit of either E or H polarization, however, Y_F becomes identically zero. Hence, the perpendicular beam displacement does not arise in the theory of the *Goos-Hänchen* effect, presented above.

Unlike D of (62), Y_F does not vanish in the region of partial reflection, but its magnitude is generally small. It assumes a maximum at the critical angle for total reflection, too; but this angle must probably be excluded from calculation for the same reason. Bearing this fact in mind, the reader is referred to *Schilling's* papers ([18] and [23b]) for a detailed discussion of the perpendicular beam displacement Y_F .

5.2 Total Reflection of Converging and Diverging Beams

Mintop's discovery of an advanced response in seismic shock phenomena [59] was later explained by *v. Schmidt* [25] on the basis of a conical wavefront, the so-called *v. Schmidt's lateral wave*. Such a wavefront arises in the total reflection of a diverging wave due to the propagation-velocity difference in the adjacent media. This intuitive interpretation initially encountered some resistance in the scientific community (see, e.g., [60]), in particular since even *Sommerfeld* did not immediately recognize the physical connection to his earlier work [61]. Only after *v. Schmidt* [62] could demonstrate, by means of Schlieren photographs [51], a series of acoustical spark experiments, was his physical interpretation appreciated and finally cast into mathematics by *Joos* and *Telhou* [63] and others [64], but especially by *Oh* [65]. The translation of *v. Schmidt's* lateral wave into optics was first achieved by *Maecker* [17], who also pointed out its connection with the *Goos-Hänchen* effect.

The reflection of a diverging wave at the interface toward an optically less-dense medium is schematically illustrated in Fig. 16a. A spherical wave expanding about its point source at Q is reflected and refracted from the same contour along the interface if intersecting the interface at an angle less than the critical angle for total reflection. At the critical angle, the refracted

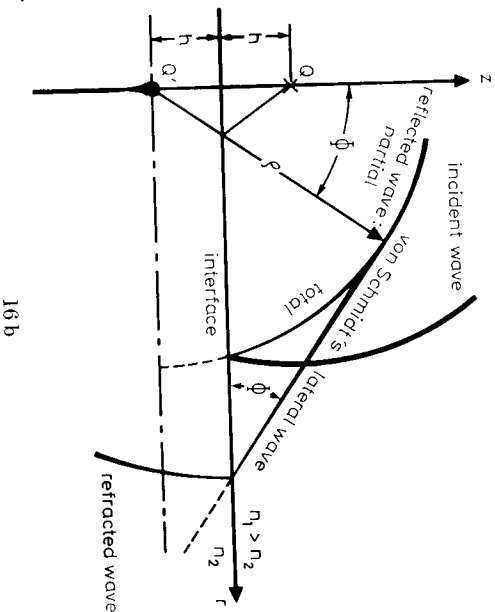
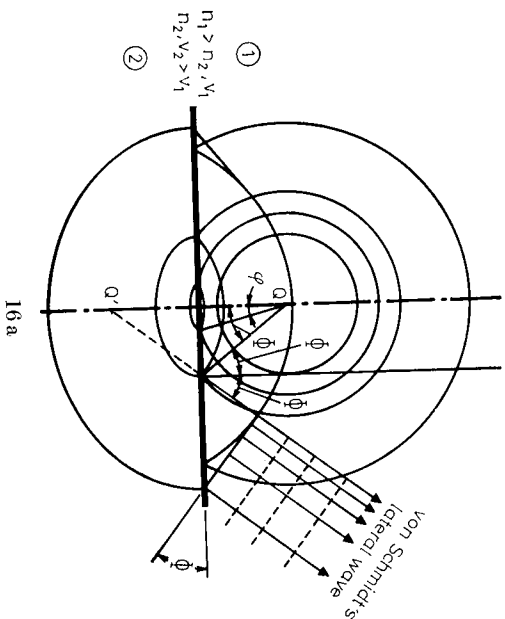


Fig. 16. Illustrating the total reflection of a diverging wave. Figure (a) explains the physics of reflection and refraction at an interface between two media with different velocities of propagation. Von Schmidt's lateral wave is, for simplicity, indicated only on the right-hand side. Figure (b) defines the notation for the mathematical description. The comet-shaped image Q' visualizes *Maaecker's* interpretation of v. Schmidt's lateral wave, [17]. (Reproduction through the courtesy of H. Maaecker, TH Munich, Germany.)

wavefront is perpendicular to the interface since $\varphi_2 = 90^\circ$. As time, and thus the angle of incidence, increase further, the refracted wave in the less-dense medium propagates faster than the reflected wave in the denser medium. The continuity of the electromagnetic field across the interface requires the appearance of a conical wavefront connecting tangentially the reflected wave with the intersection of refracted wave and interface. This conical wavefront represents v. Schmidt's lateral wave. It intersects the interface at the Mach angle [49] which is equal to the critical angle for total reflection. The rays of light are the orthogonal trajectories to the wavefront, as indicated in Fig. 16a, and therefore encounter the interface at the critical angle.

The foregoing discussion is now supplemented by the final results of *Ohl's* derivation [65b]. A dipole making the angle Θ with the z axis is located in the denser medium at the distance h above the $z = 0$ interface, as illustrated by Fig. 16b. We adopt simultaneously the cylindrical (r, φ, z) and spherical $(\varrho, \varphi, \beta)$ coordinates; the latter system being centered at the image point Q' of the source dipole Q , namely at $z = -h$. The plane of incidence is the zr plane which makes the angle β with the zx plane. In optics the reflected spherical wave is given, using the spherical coordinates, by its electric field strength

$$E_{\perp} r = -A_{\perp} k^2 \sin \Theta \sin \beta R_{\perp}(\varphi) e^{ik\varrho} / \varrho \quad (64a)$$

for E polarization and

$$E_{\parallel} r = -A_{\parallel} k^2 [\cos \Theta \sin \varphi + \sin \Theta \cos \varphi \cos \beta] R_{\parallel}(\varphi) e^{ik\varrho} / \varrho \quad (64b)$$

for H polarization, where the amplitude factors A_{\perp} and A_{\parallel} are used as in (4) and (6). The quantities $R_{\perp}(\varphi)$ and $R_{\parallel}(\varphi)$ denote Fresnel's formulas (13a) and (16a), respectively. The corresponding expressions for v. Schmidt's lateral wave can be written in cylindrical coordinates, assuming $\varphi > \Phi$, as

$$e_{\perp} = -i2A_{\perp} k \frac{\tan \Phi}{\cos \Phi} \sin \beta \frac{e^{ikr} \sin \vartheta + (z+h) \cos \vartheta}{r^2 (1 - \cot \eta \varphi \tan \Phi)^{3/2}} \quad (65a)$$

and

$$e_{\parallel} = -2A_{\parallel} k \frac{(\cos \Theta \sin \Phi + \sin \Theta \cos \Phi \cos \beta)}{\sin \Phi \cos^2 \Phi} \frac{e^{ikr} \dots}{r^2 (\dots)^{3/2}} \quad (65b)$$

Attention is directed to the significant fact that v. Schmidt's lateral wave is determined by the location of the image point Q' since z appears only in the form $(z+h)$. That is to say, it is independent of the position of both the interface and the dipole itself. Strictly speaking, the source dipole produces a comet-shaped rather than a point image on account of v. Schmidt's lateral wave, as indicated in Fig. 16b, [17].

The intensity of v. Schmidt's lateral wave is nonuniform, decreasing continuously along the conical wavefront for $(\Phi < \varphi \leq 90^\circ)$. This intensity distribution and the complementary one of the refracted wave due to the energy leakage are indicated in Fig. 16b by the variable thicknesses of the

curves. It should be noted that the ratio $|E_{\perp}/E_{\parallel}| = n^2$ is constant along the conical wavefront ([17] and [65b]).

Ohl [65a] showed that, as the source dipole approaches the interface, the theory of v. Schmidt's lateral wave is consistent with the classical problem of an electric dipole above a lossy (conducting) half-space ([61b] and [66]). In fact, he clearly recognized the significance of v. Schmidt's lateral wave as ground wave in the propagation of electromagnetic energy above the earth [67]. This topic has meanwhile been treated extensively in the literature [68]. Similar wave phenomena can arise in optics if a surface wave is disturbed by a dust particle or if the incident beam is tangent to a curved surface [17].

Maueker ([17] and [69]) advanced the ray-tracing approach of geometrical optics and arrived at results which contain more information than *Ohl*'s electromagnetic theory of second order [65a]. In particular, he investigated the physical connection between v. Schmidt's lateral wave and the *Goos-Hänchen* effect. The basic idea of his approach is now sketched briefly, assuming a glass/air interface with $n = 1/1.52$. A diverging wave can be visualized by radial rays emanating from a localized source. These rays encounter the interface at varying angles, as shown in Fig. 17. Their total reflection is determined by two processes which are, in part, counteracting. Firstly, the point of incidence moves at the interface according to $h \cdot \tan \theta$; as the angle of incidence increases; and secondly, there is a shift of the reflection center due to the *Goos-Hänchen* effect. Accordingly, we obtain the ray pattern depicted in Fig. 17. We see that the rays intersecting the interface near the critical angle for total reflection produce v. Schmidt's lateral wave with its conical wavefront, all others contribute to the reflected wave with its curved wavefront. The corresponding ray pattern for a converging wave is exhibited in Fig. 18; we note the absence of v. Schmidt's lateral wave. In summary, *Maueker*'s investigations reveal the important conclusion that v. Schmidt's lateral wave arises if and only if the incident wave is diverging. This conclusion reiterates the significance of a real source at finite distance and hence excludes converging and parallel beams.

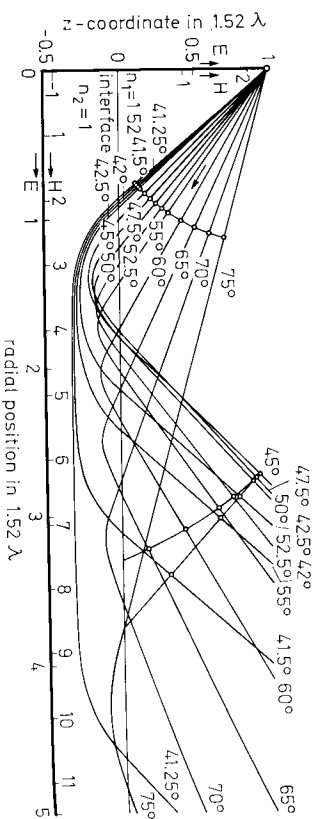


Fig. 17. Illustrating the total reflection of a diverging wave with ray tracing of geometrical optics to demonstrate the occurrence of v. Schmidt's lateral wave. [17]. The dipole source is assumed at unit distance in the case of E_z polarization. (Reproduction through the courtesy of H. Maueker, TH Munchen, Germany.)

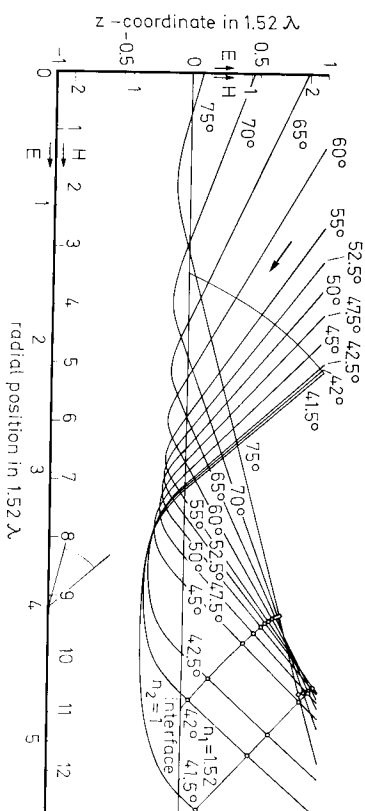


Fig. 18. Illustrating the total reflection of a converging wave with ray tracing of geometrical optics to demonstrate the absence of v. Schmidt's lateral wave. [17]. The dipole source is assumed at unit distance in the case of E_z polarization. (Reproduction through the courtesy of H. Maueker, TH Munchen, Germany.)

An outgrowth of *Maueker*'s investigation [69a] was the observation that the image of a totally-reflected point source should be a toroid rather than a point. This observation could be substantiated by experiment [69c].

The general problem of total reflection, based upon either a cylindrical or a spherical wave, was undoubtedly treated by more than the above cited investigators. *Picht* [60] initially related v. Schmidt's lateral wave to a particular solution of his earlier treatment. He later summarized his extensive research in monograph form [70]. *Schilling* [71] extended *Picht*'s work to the case of absorbing media. This case has an important application in the propagation of electromagnetic waves along the earth. *Ohl* [67] pointed out that the flow of energy into the earth is a prerequisite for v. Schmidt's lateral wave within the earth: the absorption of the earth plays a role of second order. In the limit as the earth becomes perfectly conducting, v. Schmidt's lateral wave vanishes. *Tannir* and *Oliver* [26] considered the other special case of an absorbing denser medium. Here, v. Schmidt's lateral wave may carry more energy to an observer than the reflected wave since part of its path is taken through the nonabsorbing less-dense medium. The existence of lateral waves in slab configurations was discussed by *Tannir* and *Felsen* [72]. The reader is referred to *Brekhovskikh*'s book for a very lucid exposition of the theory under consideration [30c]. Its application to acoustics was extensively reviewed by *Schoch* [22a].

5.3 Total Reflection of a Parallel Beam with Diffraction

Up to this point, the amplitude distribution $A(\beta)$ of the incident beam has been assumed to be real on account of (3). This assumption, although reasonable in the description of the classical *Goos-Hänchen* effect, encounters some difficulty when the theory presented in Chapter 1 is to be extended to higher order. Rather than proceeding along a mathematically cumbersome route we advance a physical interpretation for the total reflection of a parallel beam

with diffraction. We assume that a beam with the amplitude distribution illustrated by Fig. 4a has been formed by transmitting a plane wave through an aperture. Diffraction thus introduced may be visualized by a parallel beam-field with diffraction waves superimposed. The latter are secondary (cylindrical or spherical) wavelets "scattered" at the diffracting edge of the aperture. — Such a field decomposition into diffraction and geometrical-optical waves, originally suggested by Young [73], Maggi [74], and Sommerfeld [47], represents a well-established concept in scalar diffraction theory [75], as well as in its rigorous electromagnetic form [76]. — These wavelets have comparatively small, but nonvanishing amplitudes and can be demonstrated, at least, in the border zones of the parallel beam. Since they are diverging, they generate v. Schmidt's lateral wave in total reflection according to the preceding section. Hence, when a parallel beam with diffraction is totally reflected, the dominant *Goos-Hänchen* effect is accompanied by v. Schmidt's lateral wave as a second-order phenomenon. This phenomenon produces the appearance of illumination trailing the totally reflected beam, as observed by *Acloque* and *Guillemet* [77], and *Osterberg* and *Smith* [78]. The latter investigators performed a series of ingenious and detailed experiments for a better understanding of the problem. In particular, they observed a sharp maximum of the trailing illumination at an angle of incidence which is between 1–2 sec below the critical angle for total reflection in most cases. This observation lends additional support to the above interpretation, since diffraction introduced by the limiting aperture produces a deviation in this order of magnitude.

The above interpretation is directly applicable to the clever experiment in which *Maeker* [17] first demonstrated v. Schmidt's lateral wave in optics. It also represents the essential idea of the *Tamir* and *Oliver* paper [26], although not expressed clearly. This paper provides a plausible explanation of the illumination-trailing phenomenon ([77] and [78]), referred to above. Attempts to describe this phenomenon with rigor [79] have not produced numerical results to date.

Recent experiments on v. Schmidt's lateral wave induced by a laser beam at a liquid/air interface provide some measurements on the lateral-wave propagation and attenuation, [80]. The dependence upon polarization seems in fair agreement with the prediction of Section 5.2.

The foregoing discussion is strongly supported by an experimental observation noted in acoustics but unexplained so far ([Ref. 30, Fig. 12], [50a, b] and [81]). A sharp dip is seen in the functional dependence of the reflectivity, at a liquid/solid interface, versus the angle of incidence near the critical angle for total reflection. This phenomenon, which cannot be explained on the basis of the familiar plane-wave theory, may be traced to the excitation of v. Schmidt's lateral wave. Its interpretation becomes still more apparent

¹³ We know very well from our daily experience that edges of illuminated objects shine when observed from their shadow, as already noticed by *Newton* [Ref. 2, Book 3, Observations V and VI]. Under *Newton's* assumption the diffracting edge exerts forces on the light corpuscles passing in its neighborhood. Thus, the diffracted light is, so to speak, generated by a scattering process of the incident light on the diffracting edge.

when noting that the incident beam used in the measurement had a small (about 3°) divergence. This case may even be considered the other extreme of a parallel beam with diffraction, namely where the diffraction wave is dominant. — The excitation of Lamb's waves briefly mentioned in Section 4.1 is responsible for the fine structure in the measurements on aluminum plates, reported by *Weinstein* [81].

(To be continued)

53. $(0\mathfrak{s}')_{\nu} = (0\mathfrak{s})_{\nu} \cdot (\mathfrak{s}'x)_{\nu} + (0\mathfrak{s})_{\nu} \cdot (\mathfrak{s}'y)_{\nu} + (0z)_{\nu} \cdot (\mathfrak{s}'z)_{\nu}$
54. $u_{\nu+1} = r_{\nu} \cdot (0\mathfrak{s}')_{\nu} + k_{\nu+1} \cdot (\mathfrak{s}'z)_{\nu}$
55. $(0\mathfrak{s}')^2_{\nu+1} = \frac{u_{\nu+1} \cdot u_{\nu+1} + 1 \cdot v_{\nu+1} + 2k_{\nu+1} \cdot z_{\nu}}{r_{\nu+1}^2}$
56. $(0\mathfrak{s})_{\nu+1} = + \sqrt{(0\mathfrak{s})_{\nu+1}^2}$
57. $\tilde{d}'_{\nu} = 1 \cdot u_{\nu+1} - r_{\nu+1} \cdot (0\mathfrak{s})_{\nu+1}$
58. $x_{\nu+1} = \tilde{d}'_{\nu} \cdot (\mathfrak{s}'x)_{\nu} + x_{\nu}$
59. $y_{\nu+1} = \tilde{d}'_{\nu} \cdot (\mathfrak{s}'y)_{\nu} + y_{\nu}$
60. $z_{\nu+1} = \tilde{d}'_{\nu} \cdot (\mathfrak{s}'z)_{\nu} + z_{\nu} - k_{\nu+1}$
61. $(\mathfrak{s}x)_{\nu+1} = (\mathfrak{s}'x)_{\nu}$
62. $(\mathfrak{s}y)_{\nu+1} = (\mathfrak{s}'y)_{\nu}$
63. $(\mathfrak{s}z)_{\nu+1} = (\mathfrak{s}'z)_{\nu}$
- (Die Teile III und IV folgen)

Beam Displacement at Total Reflection: The Goos-Hänchen Effect, IV*

By Helmut K. V. Lotsch**

Institut für Theoret. Elektrotechnik, TU Aachen, Germany

Received 1 April 1970

Abstract

The paper is divided into four parts. Part I comprises the Introduction and the two chapters entitled "Reflection and Refraction of a Beam of Light" and "Total Reflection of an E-Polarized Beam". Part II treats the *Goos-Hänchen* effect in classical optics. The different descriptions are discussed and their results are compared with *Waller's* measurements. Part III deals with the *Goos-Hänchen* effect in other branches of physics such as acoustics, quantum mechanics, plasma physics and nonlinear optics. The Schöch effect is introduced; furthermore the total reflection of diverging and converging waves is investigated. The final Part IV is devoted to several applications of the *Goos-Hänchen* effect, including the case of absorbing media. In addition, it contains the Summary and Conclusion, and the extensive list of references.

Inhalt

Strahlversetzung bei der Totalreflexion. Die vorliegende Arbeit ist in vier Teile unterteilt. Teil I umfaßt die Einleitung und die beiden Kapitel „Reflexion und Brechung eines Lichtstrahles“ und „Totalreflexion eines E-polarisierten Lichtstrahles“. Teil II behandelt den *Goos-Hänchen*-Effekt in der klassischen Lichtverschiedenen Beschreibungen werden besprochen und ihre Ergebnisse mit den Messungen von *Waller* verglichen. Teil III befaßt sich mit dem *Goos-Hänchen*-Effekt in anderen Zweigen der Physik, nämlich der Akustik, der Quanten-Mechanik, der Plasma-Physik und der nichtlinearen Optik. Der Schöch-Effekt wird eingeführt; ebenso wird die Totalreflexion divergierender und konvergierender Wellen untersucht. Der abschließende Teil IV ist einigen Anwendungen des *Goos-Hänchen*-Effektes, einschließlich dem Fall absorbierender Medien, gewidmet. Außerdem enthält er die Zusammenfassung und Schlussbetrachtung und das ausführliche Literaturverzeichnis.

6. Application and/or Utilization of the Goos-Hänchen Effect

This chapter is concerned with several cases in which the *Goos-Hänchen* effect is either applied or utilized. The discussion of each case is necessarily brief in order to stay within the scope of the present paper, but the reader will find ample references to pertinent literature. Our point of departure is

* Dissertation approved by the Faculty of Electrical Engineering at the T. U. of Aachen, translated into English. Part I-III: *Optik 32* (1970), 116, 189, 299.

** Author's address: Autometrics Division of North American Rockwell, Anaheim, California 92803.